INSTITUTE OF PHYSICS PUBLISHING JOURNAL OF PHYSICS B: ATOMIC, MOLECULAR AND OPTICAL PHYSICS

J. Phys. B: At. Mol. Opt. Phys. **38** (2005) 4349–4361 doi:10.1088/0953-4075/38/24/002

Collisional and thermal ionization of sodium Rydberg atoms III. Experiment and theory for nS and nD states with n = 8–20 in crossed atomic beams

I I Beterov[1], D B Tretyakov[1], I I Ryabtsev[1], N N Bezuglov[2], K Miculis[3], A Ekers[3] and A N Klucharev[2]

[1] Institute of Semiconductor Physics, Department of Quantum Electronics, 630090 Novosibirsk, Russia
[2] St. Petersburg State University, Fock Institute of Physics, 198904 St. Petersburg, Russia
[3] University of Latvia, Institute of Atomic Physics and Spectroscopy, LV-1586 Riga, Latvia

E-mail: beterov@isp.nsc.ru

Received 8 August 2005, in final form 25 October 2005
Published 28 November 2005
Online at stacks.iop.org/JPhysB/38/4349

Abstract

The results of experimental and theoretical studies of collisional ionization of Na Rydberg atoms in nS and nD (n = 8–20) states are presented. Molecular and atomic ions from associative ionization and photoionization by blackbody radiation were detected after pulsed laser excitation of Rydberg states in crossed Na atomic beams. An original method of determination of associative ionization rate constants based on the measurement of ratios of molecular and atomic ion signals was used, which did not require the determination of absolute number density of Rydberg atoms. The measured rate constants of associative ionization of Rydberg atoms in collisions with ground-state Na atoms are compared with the results of our earlier single-beam experiment and theoretical calculations. It is shown that the stochastic ionization model, which describes the collisional ionization of Rydberg atoms in terms of chaotic migration of highly excited electron induced by the motion of the colliding nuclei, yields a significantly better agreement with the experimental results than the earlier Duman–Shmatov–Mihajlov–Janev model.

1. Introduction

Our previous experimental [1] and theoretical [2] articles, hereafter referred to as papers I and II, respectively, reported on associative ionization (AI) of sodium Na(nL) Rydberg atoms in nS and nD states in collisions with ground-state Na(3S) atoms and on photoionization by room-temperature blackbody radiation (BBR):

$$\mathrm{Na}^{**}(nL) + \mathrm{Na}(3\mathrm{S}) \rightarrow \mathrm{Na}_2^+ + e \qquad \text{associative ionization,} \tag{1}$$

$$\mathrm{Na}^{**}(nL) + \hbar\omega_{\mathrm{BBR}} \rightarrow \mathrm{Na}^+ + e \qquad \text{BBR photoionization.} \tag{2}$$

Paper I reported on experimental measurements of AI rate constants for the process (1) in a single effusive atomic beam. The measurements were performed for Rydberg states with principal quantum numbers $n = 8$–20 and the results were compared with those of other studies of Na collisions. In paper I it was also shown that photoionization by BBR is the main source of Na^+ ions at excitation of Rydberg states in single Na beams at atom number densities of 5×10^{10} cm^{-3} and ambient temperatures of 300 K. The contribution of Penning-type collisional ionization[4], in which atomic ions are formed instead of the molecular ions, to the observed Na^+ signal was negligible. This allowed us to use the Na^+ signal for calibration of the collisional ionization rate without the measurement of lifetimes and number densities of Rydberg atoms. The measurements of the latter are typically associated with large experimental uncertainties for states with $n < 20$, because the commonly used field ionization technique [3] would require short electric field pulses as strong as 30 kV cm^{-1} for $n \sim 10$, which are difficult to obtain and handle, while other techniques lack the desired accuracy.

In paper II, the stochastic model (SM) describing the AI process in collisions of ground-state atoms with Rydberg atoms was presented. Like the earlier Duman–Shmatov–Mihajlov–Janev (DSMJ) model [4–6], SM treats the pair of colliding atoms as evolution of a highly excited quasi-molecule, temporarily formed in the collision. The nuclei periodically exchange with the inner valence electron that generates a quasi-monochromatic radiation field. This field can be absorbed by the Rydberg electron, leading to photoionization of the quasi-molecule and stabilization of the colliding pair as a molecular ion. The key difference between the SM and the DSMJ model is that the former takes into account random migration of the outer electron over a range of Rydberg states prior to ionization whereas the latter ignores it. Such migration occurs due to non-adiabatic transitions at numerous crossings of energy levels of the highly excited quasi-molecule. In contrast, the DSMJ model relies on assumption that the initially excited Rydberg state does not change in course of the collision until the very ionization.

Notable disagreement between the AI rate constants measured under single beam-conditions in paper I and the theoretical rate constants calculated using the SM (paper II) and DSMJ model was observed for relatively low principal quantum numbers $8 < n < 12$, at the same time, the results of an earlier crossed-beams experiment with $Na^{**}(n\mathrm{P})$ atoms by Boulmer *et al* [8] are in good agreement with the results of SM. A possible explanation of such differences is related to the fact that collision energies in single beams are by an order of magnitude lower than those in crossed beams at the same source temperatures. We therefore concluded that disagreement of the theory with the single beam data may be due to the perturbation of nuclear motion by the stochastic behaviour of Rydberg electron in course of the collision, which is likely if the collisions are sufficiently slow. Such perturbations were disregarded in the calculations of paper II. Unfortunately, [8] is the only crossed-beam experiment on AI of Na Rydberg atoms reported so far. The present study is focused on obtaining the missing AI rate constants for sodium nS and nD states in a crossed-beam experiment at relatively high (thermal) collision energies. Such data are essential for the assessment of validity of the stochastic ionization model presented in paper II.

This paper is organized as follows. Section 2 describes the experimental setup and time-of-flight measurements of longitudinal velocity distributions of the effusive atomic beams. Section 3 presents the measurements of AI rate constants for sodium nS and nD states in two crossed beams, using the BBR photoionization signal as a reference. Section 4 presents the

[4] Although the term Penning ionization was initially introduced to describe the formation of atomic ions in heteronuclear collisions of excited atoms [7], we follow the authors of [8] and use this term for the more general case of the formation of atomic ions in both homonuclear and heteronuclear collisions, as opposed to the molecular ion formation in homonuclear and heteronuclear collisions, which is termed associative ionization.

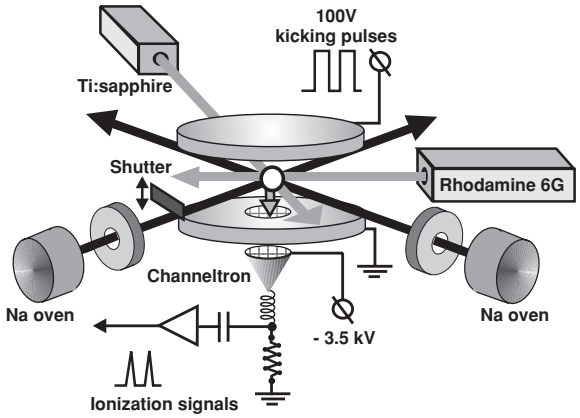

Figure 1. Experimental arrangement of the atomic and laser beams, and the ion detection system.

experimental AI rate constants and provides a comparison with the theory. The results and conclusions are summarized in section 5.

2. Experiment

2.1. Atomic beams and laser excitation

The experimental setup and laser excitation scheme were described in detail in paper I. The second effusive sodium beam source, identical to the first one, has been added to perform measurements of AI rate constants in crossed atomic beams (figure 1). The atomic beams were formed by expansion of sodium vapour through 2 mm dia openings in both ovens, which were kept at the temperature of 600 K. Both beams were collimated by 1.5 mm apertures positioned at the distance of 5 cm from each opening. The beams crossed at right angles at the distance of 9 cm from the openings. In the crossing (i.e., reaction) zone of both beams, the atoms were excited to nS and nD states with $n = 8$–20 in two steps using pulsed laser radiation resonant with the $3S_{1/2} \rightarrow 3P_{3/2}$ and $3P_{3/2} \rightarrow nL$ transitions. The transverse spatial distribution of atoms in each beam in the reaction zone was measured by observing the image of resonant fluorescence at 589 nm induced by the first-step excitation laser. The measured profiles were symmetrical trapezoids with 1 mm vertex and 4 mm base, well coinciding with geometrical calculations for effusive beams. A mechanical shutter could interrupt one of the beams in order to switch between measuring the fluorescence and ionization signals from a single beam or from crossed beams.

As in paper I, the present study is focused on the measurement of relative dependence of ionization rate constants on the principal quantum number n of Rydberg states. In order to determine the absolute rate constant values, the number density n_{3S} of ground-state Na(3S) atoms was calculated from the geometry of both atomic beams and the formula of Browning and Potter [9] relating temperature and pressure of saturated Na vapour in the beam sources. By monitoring resonance fluorescence signals we verified that the atomic number density was almost constant during the experiments. Taking into account all uncertainties, we estimate the average number density of atoms in the reaction zone to be $n_{3S} = (4 \pm 1) \times 10^{10}$ cm^{-3} at the temperature of both beam sources of $T_{\mathrm{bs}} = (600 \pm 2)$ K.

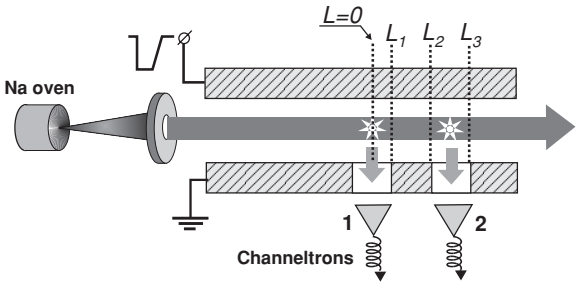

Figure 2. Schematic arrangement of the detection system for time-of-flight measurements of the velocity distribution in a single atomic beam.

2.2. Measurement of velocity distribution

In paper II and in an earlier theoretical study [10] it was shown that variations in relative collision velocity distributions of the colliding atoms strongly affect the values of measured and calculated AI rate constants and thus influence their dependences on principal quantum number. The shape of the rate constant n dependence results from averaging the velocity-dependent reaction cross-section over the velocity distribution of the given experiment. The idealized theoretical velocity distributions, which are usually used in calculations, may differ from the experimental ones. In paper II we calculated the AI rate constants using the theoretical relative velocity distribution from our earlier study [11], assuming that atomic velocities along the beam axis follow the Maxwell distribution:

$$f(v) = \frac{4}{\sqrt{\pi}} \frac{v^2}{v_0^3} \exp\left(-v^2/v_0^2\right), \tag{3}$$

where v is the velocity of atoms along the beam axis, $v_0 = \sqrt{2T/m}$, T is the temperature of the beam source in atomic units, and $m = 42\,228$ au is the mass of Na atom.

In order to verify whether equation (3) correctly describes the velocity distributions of atoms in our effusive beams, we performed special time-of-flight measurements. We used the same setup as shown in figure 1, with modifications shown in figure 2. The lower electrode of the reaction chamber was equipped with an additional 6 mm dia opening covered by mesh, and an additional channeltron (C2) was placed under this opening to enable the detection of electrons that are created above it. The central opening and the channeltron (C1) were located below the crossing point of laser and atomic beams. They were used for measurements of the AI rate constants. The axis of the second opening and of the channeltron (C2) were both located at 17 mm downstream one of the atomic beams. Such arrangement of C1 and C2 enabled the time-of-flight velocity measurements of atoms in the beam.

Sodium atoms were excited to the 37S Rydberg state at time $t = 0$ by a 50 ns laser pulse focused on the atomic beam above the centre of C1. The focal point of the laser defines the $L = 0$ coordinate along the atomic beam axis. The advantages of using high Rydberg states with $n \sim 40$ for time-of-flight measurements are related to their long lifetimes and low critical fields required for their detection by selective field ionization (SFI) technique [3]. The critical field for the 37S state is about 200 V cm^{-1}. After the excitation, Rydberg atoms propagated downstream the beam. After a variable delay time t with respect to the laser pulse, a 3 μs electric field pulse of 300 V cm^{-1} was applied. This pulse ionized all atoms in the 37S state and in nP states with $n > 33$. The latter were populated by spontaneous and BBR-induced transitions from the initially excited 37S state. The electrons produced by field ionization

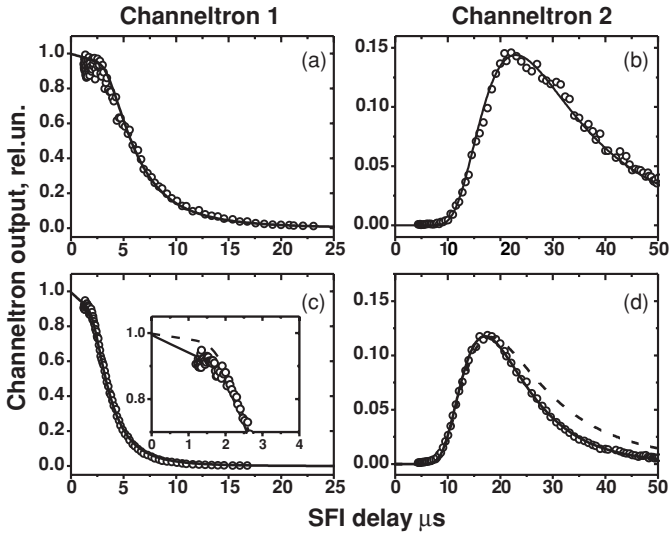

Figure 3. Experimental and theoretical dependences of channeltrons' signals $N_1(t)$ and $N_2(t)$ on the delay time t of the ionizing SFI pulse: (a) and (b) are signals of C1 and C2, respectively, for low-density (3×10^6 cm^{-3}) atomic beam at the source temperature of 420 K; open circles—experiment, full curves—theory with $\tau_{\text{eff}} = 58$ μs; (c) and (d) are signals of C1 and C2, respectively, for dense atomic beam (4×10^{10} cm^{-3}) at the source temperature of 630 K; open circles—experiment, full curves—theory with $\tau_{\text{eff}} = 18$ μs; broken curves—theory with $\tau_{\text{eff}} = 58$ μs.

above C1 and C2 were immediately guided to the respective channeltron by the electric field pulse and detected.

At time t after the laser pulse, all atoms with velocities within the ranges $(0, L_1/t)$ and $(L_2/t, L_3/t)$ are located above C1 and C2, respectively. The corresponding distances are $L_1 = 3$ mm, $L_2 = 14$ mm and $L_3 = 20$ mm (figure 2). Time evolution of the total population of atoms in the 37S and in nP ($n > 33$) states is given by the effective lifetime τ_{eff}. We calculated τ_{eff} to be 58 μs at the ambient temperature of 300 K. The numbers of Rydberg atoms detected at the moment t by C1 and C2 are given by the following expressions (normalized to the unity total number):

$$N_1(t) = \int_0^{L_1/t} f(v) \exp(-t/\tau_{\text{eff}})\, \mathrm{d}v, \tag{4}$$

$$N_2(t) = \int_{L_2/t}^{L_3/t} f(v) \exp(-t/\tau_{\text{eff}})\, \mathrm{d}v, \tag{5}$$

where $f(v)$ is the velocity distribution of atoms along the beam axis. Comparison between the signals measured by C1 and C2 and the numbers of atoms calculated using equations (4) and (5), respectively, allowed us to draw the following conclusions about the velocity distribution of atoms in the beam.

At the low beam source temperature of $T = 420$ K, which corresponds to a low-density beam with 3×10^6 cm^{-3} atoms in the reaction zone, equations (4) and (5) well described the experimental observations, when the calculated effective lifetime of 58 μs and the velocity distribution (3) were used in the calculations (figures 3(a) and (b)). Hence, at low densities the velocity distribution is well described by equation (3), and the 37S state decays only via spontaneous and BBR-induced transitions.

At the higher source temperature of 630 K, which produces a dense (4×10^{10} cm^{-3}) atomic beam, the signals measured by C1 and C2 could be well reproduced if the velocity distribution (3) and effective lifetime of 18 μs were used in equations (4) and (5) (full curves in figures 3(c) and (d)). Calculations with $\tau_{\rm eff} = 58$ μs yielded a noticeable disagreement with experiment (broken curves in figures 3(c) and (d)). Any attempts to achieve an agreement by varying the velocity distribution failed if $\tau_{\rm eff} = 58$ μs was kept unchanged. This means that the absolute velocity distribution in the dense beam was still close to the Maxwell distribution, but an additional quenching term with the rate of about 40 000 s^{-1} had appeared in the total decay rate of the 37S state. Such quenching can only be caused by more frequent collisions with ground-state Na atoms, because the conditions of measurements of figures 3(a)–(d) are identical except for increased source temperature and increased number density of Na atoms in the latter case. Collisions with background gases in the vacuum chamber can be ruled out, since they would affect lifetimes in both high-density and low-density atomic beam, which was not the case. The supposed quenching in collisions with ground-state atoms is facilitated by the relatively large geometric cross-section 4.1×10^{-10} cm^2 of atoms in the 37S state (calculated using equation (42) of paper II). The quenching rate of 40 000 s^{-1} corresponds to the cross-section of 3×10^{-11} cm^2, which is by one order of magnitude smaller than the geometric cross-section.

Clarification of the mechanism of collisional quenching of the 37S state in the dense atomic beam is beyond the scope of this paper. It may be due to elastic scattering of Rydberg atoms out of the beam, or due to collision-induced transitions to lower Rydberg states that are not detected by the SFI pulse. Whatever is the mechanism, it does not anyhow affect our AI rate measurements performed during a short period of 2 μs with low-n Rydberg states, which have by more than one order of magnitude smaller geometrical cross-sections than the 37S state.

From the above discussion we conclude that the absolute velocity distribution of atoms in our effusive beams is close to the Maxwell distribution given by equation (3), and the relative velocity distributions used in our earlier theoretical calculations reported in paper II are valid. The theoretical rate constants presented in figure 3 of this paper were also obtained using the relative collision velocity distributions calculated assuming that the velocity distribution (3) is valid in each of the effusive beams.

3. Measurement of AI rate constants

As we have shown in paper I, our measured atomic ion signal $\mathrm{Na}^{+(\mathrm{sb})}$ for an nL Rydberg atom in a single beam (sb) is given by

$$\mathrm{Na}^{+(\mathrm{sb})} = N_{nL}^{\mathrm{sb}}(0)\, W_{\mathrm{BBR}}^{\mathrm{tot}} t_{\mathrm{eff}}. \tag{6}$$

Here, $\mathrm{Na}^{+(\mathrm{sb})}$ is the total number of registered atomic ions, $N_{nL}^{\mathrm{sb}}(0)$ is the number of initially laser-excited Rydberg atoms in the interaction volume, $W_{\mathrm{BBR}}^{\mathrm{tot}}$ is the total BBR-induced ionization rate and t_{eff} is the effective interaction time,

$$t_{\mathrm{eff}} = \tau_{\mathrm{eff}}[\exp(-t_1/\tau_{\mathrm{eff}}) - \exp(-t_2/\tau_{\mathrm{eff}})], \tag{7}$$

where τ_{eff} is the effective lifetime of the initially excited Rydberg state, t_1 and t_2 are the time moments marking the end of the first and the beginning of the second extraction electric field pulses, respectively (see the timing diagram in figure 3 of paper I; both pulses are of 100 V cm^{-1} amplitude and 250 ns duration). The first electric field pulse clears the interaction zone from any ions created by photoionization of atoms by the exciting laser pulse. The second pulse extracts the ions created during 2 μs after the first electric field pulse. These ions appear due to collisional ionization and BBR photoionization.

In paper I we have measured the values of $W_{\mathrm{BBR}}^{\mathrm{tot}}$ for $n = 8$–20 and compared them with our numerical calculations. A very good agreement between the experiment and the theory has been found for nD states, while noticeable discrepancies were observed for nS states with $n > 15$. A conclusion has been drawn that the theory of photoionization of S states is probably incorrect due to non-hydrogenic character of nS states and their large quantum defects. We therefore rely hereafter on our $W_{\mathrm{BBR}}^{\mathrm{tot}}$ data, measured in paper I and use the effective lifetimes τ_{eff} calculated numerically in paper I using the quantum defect theory.

Equation (6) was written assuming that the contribution of Penning-type collisional ionization to the measured Na^+ signals is negligible. This assumption is valid in the case of single-beam experiments at atom number densities of about 5×10^{10} cm^{-3}. In the present study, we consider crossed-beam collisions at similar total number densities. The calculations of Penning-type collisional ionization rates under crossed-beam conditions showed that equation (6) is valid also in the crossed-beam case. This has been verified experimentally by measuring the dependence of Na^+ signal on the crossed-beam number density n_{3S}^{cb} of ground-state atoms in the interaction zone. This dependence is linear, thus confirming that Penning-type ionization is negligible. The contribution from collisions with background gases can be also safely disregarded: we have verified experimentally that the variation of background pressure within the range of $5 \times 10^{-7} \leqslant P \leqslant 1 \times 10^{-6}$ Torr did not affect the measured Na^+ and Na_2^+ signals by more than 5%.

In the single-beam experiment of paper I, the total number $Na_2^{+(\mathrm{sb})}$ of the molecular ions was expressed through the single-beam AI rate constant $k_{\mathrm{AI}}^{\mathrm{sb}}$, the single-beam density n_{3S}^{sb} and the constant α. The latter accounted for the contribution of Na^+ ions to the measured Na_2^+ signals at higher n. These ions represented an unavoidable technical noise originating from Na^+ ions formed during the second electric field pulse (see paper I, figure 3)]:

$$\mathrm{Na}_2^{+(\mathrm{sb})} = k_{\mathrm{AI}}^{\mathrm{sb}} N_{nL}^{\mathrm{sb}}(0) n_{3S}^{\mathrm{sb}} t_{\mathrm{eff}} + \alpha N_{nL}^{\mathrm{sb}}(0) W_{\mathrm{BBR}}^{\mathrm{tot}} t_{\mathrm{eff}}. \tag{8}$$

In the case of identical crossed beams, equation (6) must be rewritten to account for the increase in number of initially excited atoms, $N_{nL}^{\mathrm{cb}}(0) = 2N_{nL}^{\mathrm{sb}}(0)$, due to increased number density in the interaction zone $\left(n_{3S}^{\mathrm{cb}} = 2n_{3S}^{\mathrm{sb}}\right)$:

$$\mathrm{Na}^{+(\mathrm{cb})} = N_{nL}^{\mathrm{cb}}(0) W_{\mathrm{BBR}}^{\mathrm{tot}} t_{\mathrm{eff}}. \tag{9}$$

Each Rydberg atom in crossed beams can ionize in collisions with atoms from either the same beam or from the other beam. The relative collision velocity distributions are considerably different in these two cases (see paper II). Therefore, the single- and crossed-beam collisions must be considered separately, and the resulting Na_2^+ signal is described by a sum of the respective AI rate constants:

$$k_{\mathrm{AI}}^{\Sigma} = k_{\mathrm{AI}}^{\mathrm{sb}} + k_{\mathrm{AI}}^{\mathrm{cb}}, \tag{10}$$

where $k_{\mathrm{AI}}^{\mathrm{cb}}$ is the pure crossed-beam AI rate constant, which describes only the collisions between atoms belonging to different beams.

The total number of the registered Na_2^+ ions in crossed beams is given by

$$\mathrm{Na}_2^{+(\mathrm{cb})} = \tfrac{1}{2} k_{\mathrm{AI}}^{\Sigma} N_{nL}^{\mathrm{cb}}(0) n_{3S}^{\mathrm{cb}} t_{\mathrm{eff}} + \alpha N_{nL}^{\mathrm{cb}}(0) W_{\mathrm{BBR}}^{\mathrm{tot}} t_{\mathrm{eff}}. \tag{11}$$

As in paper I, we measured the ratio R^{sb} of the Na_2^+ and Na^+ signals. A formula describing R^{sb} in a single beam is obtained by dividing equation (6) by equation (8); it is independent of the values of $N_{nL}^{\mathrm{cb}}(0)$, τ_{eff} and t_{eff}:

$$R^{\mathrm{sb}} = \frac{\mathrm{Na}_2^{+(\mathrm{sb})}}{\mathrm{Na}^{+(\mathrm{sb})}} = \frac{k_{\mathrm{AI}}^{\mathrm{sb}} n_{3S}^{\mathrm{sb}}}{W_{\mathrm{BBR}}^{\mathrm{tot}}} + \alpha, \tag{12}$$

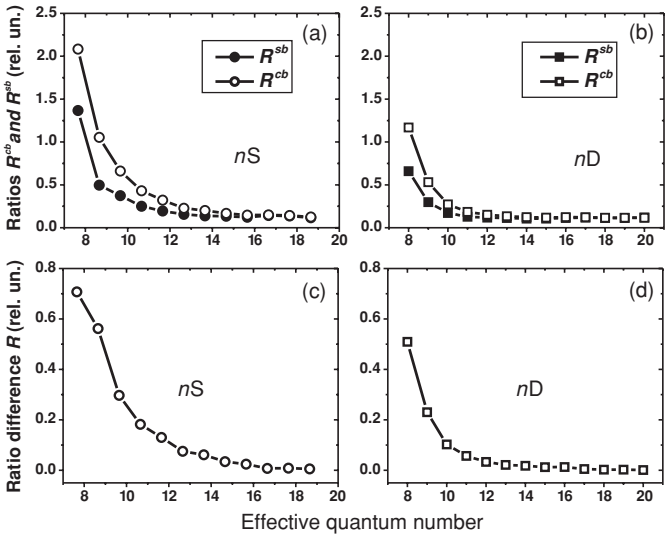

Figure 4. Experimentally measured ratios of Na_2^+ and Na^+ signals for crossed beams R^{cb} and single beam R^{sb} as a function of the effective quantum number for (a) nS states and (b) nD states; the difference of these ratios ($R^{cb} - R^{sb}$) for (c) nS states and (d) nD states, respectively.

Similarly, for crossed-beam collisions the equations (9) and (11) yield:

$$R^{cb} = \frac{Na_2^{+(cb)}}{Na^{+(cb)}} = \frac{k_{AI}^{\Sigma} n_{3S}^{cb}}{2W_{BBR}^{tot}} + \alpha. \tag{13}$$

Equation (13) allows us to determine the total rate constant as

$$k_{AI}^{\Sigma} = \frac{W_{BBR}^{tot}(R^{cb} - \alpha)}{n_{3S}^{sb}}. \tag{14}$$

It is straightforward to use equations (10) and (12)–(14) to show that the rate constant k_{AI}^{cb} is expressed through the difference ($R^{cb} - R^{sb}$), which can be directly measured in the experiment:

$$k_{AI}^{cb} = \frac{W_{BBR}^{tot}(R^{cb} - R^{sb})}{n_{3S}^{sb}}. \tag{15}$$

This expression was used to determine pure AI rate constants k_{AI}^{cb} from the measured ratios R^{cb} and R^{sb}. In contrast to the expression for k_{AI}^{sb}, which can be derived from equation (12), and the equation (14) for k_{AI}^{Σ}, the equation (15) is independent of the noise constant α. This circumstance allowed us to perform reliable measurements of the pure crossed-beam AI rate constants.

4. Results and discussion

Experimental Na_2^+/Na^+ signal ratios, averaged over five independent measurement series, are presented in figures 4(a) and (b). For the lowest states, the values of R^{sb} reach 1.3 and 0.7 for nS and nD states, respectively, while the values of R^{cb} reach correspondingly 2.1 and 1.2. All values of R decrease rapidly with increasing n until they reach a constant value of $\alpha = 0.12$ at high n, in agreement with equations (12) and (13). The difference ($R^{cb} - R^{sb}$) is shown

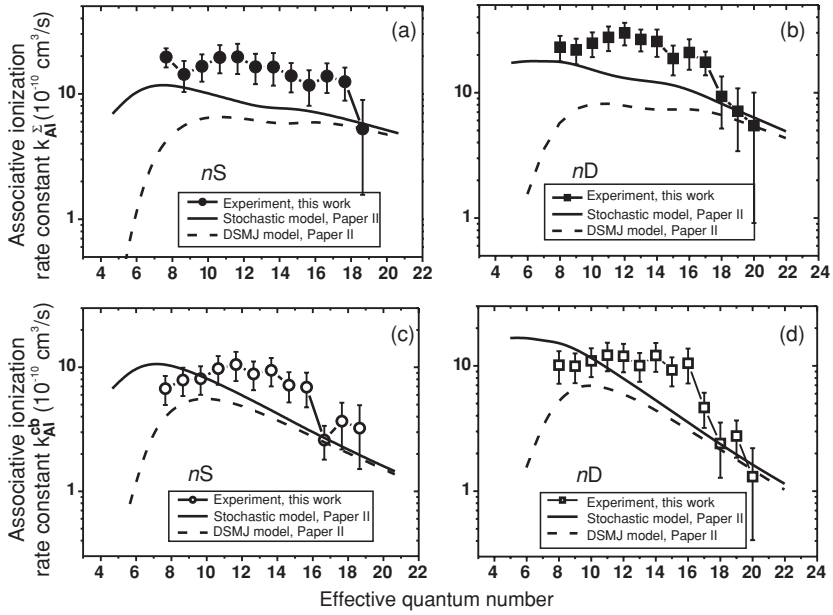

Figure 5. Experimental and theoretical $Na^{**(nl)}$ + Na(3S) AI rate constants obtained under crossed-beam conditions: (a) k_{AI}^{Σ} for nS states, (b) k_{AI}^{Σ} for nD states, (c) k_{AI}^{cb} for nS states and (d) k_{AI}^{cb} for nD states.

in figures 4(c) and (d). For the lowest states, it reaches 0.8 and 0.55 for nS and nD states, respectively, and approaches zero for high n. This confirms that the noise from Na^+ ions is really cancelled, as predicted by equation (15).

The experimental dependences of k_{AI}^{Σ} and k_{AI}^{cb} on n_{eff} (dots in figure 5) were obtained from the measured ratios R^{cb} and R^{sb} by using equations (14)–(15) and the experimental values of W_{BBR}^{tot} from paper I. The dependences of k_{AI}^{Σ} (figures 5(a) and (b)) and k_{AI}^{cb} (figures 5(c) and (d)) on n_{eff} have similar shapes, although the absolute values of k_{AI}^{Σ} are about two times larger than k_{AI}^{cb}. These dependences exhibit a wide maximum at $n_{eff} = (8–16)$ for nD states, and a narrower maximum at $n_{eff} = (11–14)$ for nS states. For higher n_{eff}, the measured values of k_{AI}^{Σ} and k_{AI}^{cb} rapidly decrease.

Figure 5 also presents the results of theoretical calculations performed using the DSMJ model (dashed lines) and the stochastic ionization model (solid lines) of paper II. The stochastic model takes into account the following physical phenomena, which are disregarded by the DSMJ model [4–6]:

(i) variation of the relative velocity distribution in single beam, crossed beam and gas cell experiments;
(ii) nonlinearity of the basic equations of DSMJ model describing the ionization of Rydberg electron;
(iii) collisional L-mixing of atoms in nD states prior to associative ionization;
(iv) 'twisting' of colliding atoms in the attractive potential due to polarization of the quasimolecular ion [12];
(v) mixing of Rydberg states by spontaneous and BBR-induced transitions;
(vi) stochastic diffusion of Rydberg electron through its energy spectrum during the collision. This diffusion occurs as the colliding atom pair undergoes numerous non-adiabatic

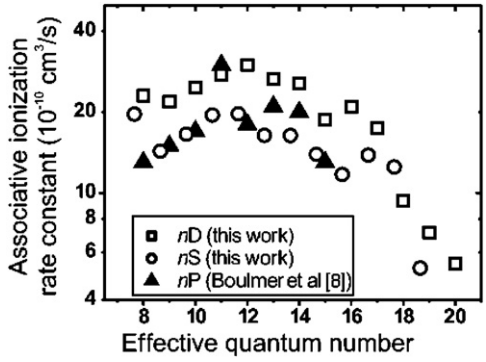

Figure 6. Comparison of the experimental associative ionization rate constants k_{AI}^{Σ} in crossed beams for nS (open circles) and nD (open squares) states measured in this work with the experimental results for nP states (solid triangles) obtained earlier in [8].

transitions in multiple overlapping crossings of the potentials of highly excited quasi-molecule in course of a single collision.

The calculations of the AI rate constants in the case of two crossed atomic beams have been carried assuming that the velocities of atoms in each beam follow the Maxwell absolute velocity distribution. The validity of such assumption is confirmed by the test described in section 2. The finite size and shape of the intersection volume of two beams was also taken into account. These two factors affect the effective interaction time since they limit the transit time of atoms through the intersection volume. Our numerical simulations have shown that these effects can be taken into account by introducing a time-dependent number density of atoms:

$$n_{3S}(t) = n_{3S}^{\mathrm{sb}} \exp(-t/\tau_f), \tag{16}$$

where $n_{3S}^{\mathrm{sb}} = 2 \times 10^{10}$ cm^{-3} is the number density of ground-state atoms at the centre of each of the beams, and τ_f is an effective time of flight (having the meaning of transit time) that was calculated to be about 2 μs for both beams. The time dependence has to be introduced in equations (44)–(49) of paper II by replacing the time-independent value of n_{3S} with $n_{3S}(t)$ given by equation (16). In contrast, in the case of head–tail collisions in a single beam the value of n_{3S} remains constant in time.

Figure 5 demonstrates that the stochastic model yields absolute values of AI rate constants that are in a substantially better agreement with the experimental data than the results of DSMJ model. At the same time, the shapes of n_{eff}-dependences of $k_{\mathrm{AI}}^{\mathrm{cb}}$ in figures 5(c) and (d) are somewhat closer to the predictions of DSMJ model.

For the sake of completeness, we compare also our experimental crossed-beams AI rate constants for nS and nD states with other data available for Na Rydberg atoms. Figure 6 shows such comparison with the results of crossed-beam experiment [8] for nP states. Both data sets appear to be similar, despite that different L-states were studied and substantially different measurement techniques were used. Importantly, in the study [8] only the total k_{AI}^{Σ} could be measured; extraction of pure crossed-beam rate constants $k_{\mathrm{AI}}^{\mathrm{cb}}$ is so far unique to our present study.

Comparison with the results of our single-beam study reported in paper I is given in figure 7. Interestingly and somewhat unexpectedly, single- and crossed-beam data turned out to be rather close to each other (especially for nD states) in contrast to the predictions of the theory of paper II for low-energy single-beam collisions. Although the mean collision velocity

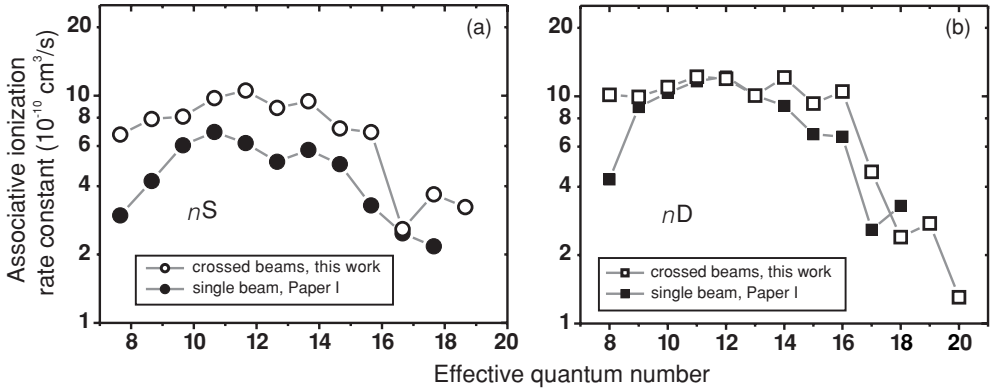

Figure 7. Comparison of the experimental associative ionization rate constants k_{AI}^{cb} for nS (open circles) and nD (open squares) states obtained in the present study for crossed beams with the experimental data on k_{AI}^{sb} for nS states (full circles) and nD states (full squares) obtained in the single beam experiment of paper I and recalculated in paper II.

is three times larger in crossed beams than in a single beam, the shapes of n_{eff}-dependences of rate constants for both nS and nD states are very similar. In addition, in the case of nD states also the absolute values are surprisingly close.

The accuracy of our measured AI rate constants in the single beam was discussed in detail in paper I. In the present study the crossed-beam rate constants k_{AI}^{cb} were determined using equation (15), therefore their accuracy depends on the accuracy with which the values of R^{cb}, R^{sb}, W_{BBR}^{tot} and n_{3S} are determined. The values of R^{cb} and R^{sb} were measured directly and they were found to be independent of laser intensity and excitation volume. The measured n_{eff}-dependences of figure 4 were reliably reproduced in several experiments. However, with increasing n_{eff} the fluctuations of $(R^{cb} - R^{sb})$ become important, because equation (15) uses the difference $(R^{cb} - R^{sb})$, which decreases rapidly with increasing n_{eff}. At the same time, W_{BBR}^{tot} grows rapidly with increasing n_{eff}. Therefore the reported values of k_{AI}^{cb} can be considered as being more reliable for $n_{eff} \leqslant 16$, while for higher n_{eff} the error in the determination of k_{AI}^{cb} is large. Note that the accuracy of the total k_{AI}^{Σ} rate constant depends also on the accuracy, with which the noise parameter α is known (see discussion in paper I). Therefore, the measurements of k_{AI}^{Σ} are less accurate than those of k_{AI}^{cb}, which are independent of α.

Another uncertainty is related to the determination of absolute value of the number density n_{3S} of ground-state atoms. In paper I we obtained the n_{3S} values from the geometry of the atomic beam using the conventional Nesmeyanov's formulae [13] relating temperature and pressure of saturated sodium vapour. However, as we later pointed out in paper II, the formula of Browning and Potter [9], which gives approximately two times higher number density at the same temperature, seems to be more reliable. It is based on careful assessment of the available experimental data, and is in a good agreement with other recent assessments (see discussion in paper II). We therefore recalculated the number density of the effusive atomic beam of paper I at $T_{bs} = 635$ K, and this recalculation increased the density value to $(5 \pm 1) \times 10^{10}$ cm^{-3}. Consequently, the absolute values of the experimental AI rate constants reported in figure 9 of paper I must be divided by a factor of 2, while the shapes of n_{eff}-dependences remain unchanged (see figure 6 of paper II).

In the present study we used the new n_{3S} values calculated from [9]. The relative values of k_{AI}^{cb} and k_{AI}^{Σ} are not affected by the absolute value of n_{3S}, since this was kept constant during the measurements. We conclude that overall absolute values of k_{AI}^{cb} and k_{AI}^{Σ} are accurate

to within better than 50% for $n \leqslant 16$, while the relative values of k_{AI}^{cb} and k_{AI}^{Σ} are accurate to within (10–20)%.

5. Conclusion

In paper I, paper II, and this work we present our results of systematic experimental and theoretical studies of associative ionization (AI) of sodium Rydberg atoms in nS and nD states with $n = 8$–20 in collisions with ground-state atoms. These results can be summarized as follows.

1. The absolute and relative values of AI rate constants have been systematically measured for the first time in single-beam and crossed-beam experiments. A novel method of determination of AI rate constants, which uses the BBR photoionization signal as a reference and does not require determination of the excitation volume and absolute number density of Rydberg atoms, has been proposed.
2. The shapes of experimental dependences of AI rate constants on the principal quantum number are similar for single and crossed atomic beams, exhibiting a broad maximum near $n_{eff} = 11$–13. The absolute values are close to the predictions of the stochastic model for the nD states, but significant differences for nS states are observed.
3. At sub-thermal energies of head–tail collisions in a single atomic beam both stochastic and DSMJ models do not correctly reproduce the shapes of experimental n_{eff}-dependences of AI rate constants. These models predict a maximum near $n_{eff} = 17$, while the experiments show a broad maximum centred at about $n_{eff} = 11$–13. Nevertheless, for $n < 15$ the stochastic model yields rate constants that are in a significantly better agreement with the experiment than the predictions of the DSMJ model.
4. At thermal energies of collisions between two crossed beams, the absolute values of total AI rate constants $k_{AI}^{\Sigma} = k_{AI}^{sb} + k_{AI}^{cb}$ and the pure AI crossed-beam rate constants k_{AI}^{cb} are better described by the stochastic model than by the DSMJ model. At the same time, the relative n_{eff}-dependences of crossed-beam rate constants k_{AI}^{cb} are somewhat better reproduced by the DSMJ model.
5. The stochastic ionization model substantially improves the conventional DSMJ model by taking into account several effects (see the list in section 4) disregarded in the latter, the most essential of which is the stochastic diffusion of Rydberg electron through its energy spectrum prior to ionization. However, the observed discrepancies between the shapes of experimental and theoretical n_{eff}-dependences of rate constants indicate that the stochastic model requires a further elaboration. In particular, the present theory does not take into account possible stochastic effects in the motion of the colliding nuclei. Such effects can lead to random changes in the electronic state of the colliding quasi-molecular system, randomly placing the nuclei in different interatomic potentials and thus randomizing the nuclear trajectories. Such randomization is expected to become particularly important in cold and ultracold atom collisions. Consideration of this kind of effects can be a subject of specific future studies.

Acknowledgments

This work was supported by INTAS project no 2001-155, INTAS Young Scientist Fellowship no 04-83-3692 (IIB), Russian Foundation for Basic Research (grants no 05-02-16181, 05-03-33252 and 05-02-16216), EU TOK project LAMOL (contract MTKD-CT-2004-014228),

European Social Fund, Latvian Science Council, NATO grant EAP.RIG.981387 (AE) and Russian Science Support Foundation (IIB).

References

[1] Ryabtsev I I, Tretyakov D B, Beterov I I, Bezuglov N N, Miculis K and Ekers A 2005 *J. Phys. B: At. Mol. Opt. Phys.* **38** S17
[2] Miculis K, Beterov I I, Bezuglov N N, Ryabtsev I I, Tretyakov D B, Ekers A and Klucharev A N 2005 *J. Phys. B: At. Mol. Opt. Phys.* **38** 1811
[3] Stebbings R F, Latimer C J, West W P, Dunning F B and Cook T B 1975 *Phys. Rev.* A **12** 1453
Ducas T, Littman M G, Freeman R R and Kleppner D 1975 *Phys. Rev. Lett.* **35** 366
Gallagher T F, Humphrey L M, Hill R M and Edelstein S A 1976 *Phys. Rev. Lett.* **37** 1465
[4] Janev R K and Mihajlov A A 1980 *Phys. Rev.* A **21** 819
[5] Mihajlov A A and Janev R K 1981 *J. Phys. B: At. Mol. Phys.* **14** 1639
[6] Duman E L and Shmatov I P 1980 *Sov. Phys. JETP* **51** 1061
[7] de Groot W and Penning F M 1933 *Handbuch der Physik* vol 23 (Berlin: Springer) p 1
[8] Boulmer J, Bonanno R and Weiner J 1983 *J. Phys. B: At. Mol. Phys.* **16** 3015
[9] Browning P and Potter P E 1985 An assessment of the experimentally determined vapour pressures of the liquid alkali metals *Handbook of Thermodynamic and Transport Properties of Alkali Metals* (Boston: IUPAC, Blackwell Scientific Publications) chapter 6.2
[10] Bezuglov N N, Borodin V M, Ekers A and Klyucharev A N 2002 *Opt. Spectrosc.* **93** 661
[11] Bezuglov N N, Klyucharev A N and Sheverev V A 1987 *J. Phys. B: At. Mol. Phys.* **20** 2497
[12] Nikitin E E and Umansky S Ya 1984 *Theory of Slow Atomic Collisions* (New York: Springer)
[13] Nesmeyanov A N 1963 *Vapour Pressure of the Chemical Elements* (London: Elsevier)
[14] Bezuglov N N, Borodin V M, Klyucharev A N, Orlovsky K V and Allegrini M 1997 *Opt. Spectrosc.* **82** 334
[15] Bezuglov N N, Borodin V M, Klyucharev A N, Fuso F, Allegrini M, Orlovsky K V and Janson M L 1999 *Opt. Spektrosc.* **86** 824
[16] Bezuglov N N, Borodin V M, Kazanskii A K, Klyucharev A N, Matveev A A and Orlovskii K V 2001 *Opt. Spectrosc.* **91** 19
[17] Ramsey N 1985 *Molecular Beams* (New York: Oxford University Press)